αII Spectrin Forms a Periodic Cytoskeleton at the Axon Initial Segment and Is Required for Nervous System Function

Claire Yu-Mei Huang, Chuansheng Zhang, Tammy Szu-Yu Ho, Juan Oses-Prieto, Alma Burlingame, Joshua Lalonde, Jeffrey Noebels, Christophe Leterrier, Matthew Rasband

Cellular/Molecular

αII Spectrin Forms a Periodic Cytoskeleton at the Axon Initial Segment and Is Required for Nervous System Function

Claire Yu-Mei Huang,[1] Chuansheng Zhang,[1] Tammy Szu-Yu Ho,[1] Juan Oses-Prieto,[3] Alma L. Burlingame,[3] Joshua Lalonde,[2] Jeffrey L. Noebels,[1,2] Christophe Leterrier,[4] and Matthew N. Rasband[1]

[1]Department of Neuroscience and [2]Department of Neurology, Baylor College of Medicine, Houston, Texas 77030, [3]Department of Pharmaceutical Chemistry, University of California, San Francisco, California 94158, and [4]NeuroCyto, NICN UMR7259, Aix Marseille Université, CNRS, 13344 cedex 15, Marseille, France

Spectrins form a submembranous cytoskeleton proposed to confer strength and flexibility to neurons and to participate in ion channel clustering at axon initial segments (AIS) and nodes of Ranvier. Neuronal spectrin cytoskeletons consist of diverse β subunits and αII spectrin. Although αII spectrin is found in neurons in both axonal and somatodendritic domains, using proteomics, biochemistry, and superresolution microscopy, we show that αII and βIV spectrin interact and form a periodic AIS cytoskeleton. To determine the role of spectrins in the nervous system, we generated *Sptan1*$^{f/f}$ mice for deletion of CNS αII spectrin. We analyzed αII spectrin-deficient mice of both sexes and found that loss of αII spectrin causes profound reductions in all β spectrins. αII spectrin-deficient mice die before 1 month of age and have disrupted AIS and many other neurological impairments including seizures, disrupted cortical lamination, and widespread neurodegeneration. These results demonstrate the importance of the spectrin cytoskeleton both at the AIS and throughout the nervous system.

Key words: ankyrin; axon; axon initial segment; cytoskeleton; node of Ranvier; spectrin

Significance Statement

Spectrin cytoskeletons play diverse roles in neurons, including assembly of excitable domains such as the axon initial segment (AIS) and nodes of Ranvier. However, the molecular composition and structure of these cytoskeletons remain poorly understood. Here, we show that αII spectrin partners with βIV spectrin to form a periodic cytoskeleton at the AIS. Using a new αII spectrin conditional knock-out mouse, we show that αII spectrin is required for AIS assembly, neuronal excitability, cortical lamination, and to protect against neurodegeneration. These results demonstrate the broad importance of spectrin cytoskeletons for nervous system function and development and have important implications for nervous system injuries and diseases because disruption of the spectrin cytoskeleton is a common molecular pathology.

Introduction

Neurons have complex cytoskeletons regulating neuronal morphology, trafficking of cargoes, and assembly of specialized membrane domains and compartments. Spectrins comprise a submembranous cytoskeleton proposed to confer strength and flexibility to the membrane (Bennett and Baines, 2001; Xu et al., 2013). Spectrins are widely expressed and exist as tetramers consisting of two α and two β subunits. There are five vertebrate β spectrins: βI–βIV are found in neurons and βV is found in hair cells (Legendre et al., 2008; Zhang et al., 2014). β spectrins are not uniformly distributed throughout cells, but are often located in specialized domains. For example, βIV spectrin forms a complex with the scaffolding protein ankyrinG (ankG) at axon initial segments (AIS) and nodes of Ranvier to cluster the voltage-gated ion channels necessary for action potential initiation and propagation (Berghs et al., 2000; Yang et al., 2007). Due to their high degree of homology, some β spectrins may compensate for one another (Ho et al., 2014). However, αII spectrin is the only α spectrin detected in the nervous system (Zhang et al., 2014), suggesting that, depending on its β spectrin binding partner, it must play important roles in a variety of cellular contexts.

Received July 26, 2017; revised Sept. 11, 2017; accepted Oct. 4, 2017.

Author contributions: C.Y.-M.H., C.Z., and M.N.R. designed research; C.Y.-M.H., T.S.-Y.H., J.O.-P., J.L., C.L., and M.N.R. performed research; C.Y.-M.H., J.O.-P., A.L.B., J.L.N., C.L., and M.N.R. analyzed data; C.Y.-M.H. and M.N.R. wrote the paper.

This work was supported by the National Institutes of Health (Grants NS044916 and NS069688 to M.N.R., Grant NS29709 to J.L.N., Grants GM103481 and 1S10OD016229-01 to A.L.B.) and the Dr. Miriam and Sheldon G. Adelson Medical Research Foundation. We thank Chih-Chuan Wang for cloning of βIVΣ1, Shelly Buffington for help with the Neurofascin affinity column, and Dr. Marie-Pierre Blanchard for help with STORM imaging. C.L. acknowledges Dr. Benedicte Dargent for support.

The authors declare no competing financial interests.

Correspondence should be addressed to Matthew N. Rasband, Department of Neuroscience, Baylor College of Medicine, One Baylor Plaza, Houston, TX 77030. E-mail: rasband@bcm.edu.

DOI:10.1523/JNEUROSCI.2112-17.2017

 0270-6474/17/3711311-12$15.00/0

Human mutations in αII spectrin cause West syndrome, a severe infantile epilepsy that includes seizures, hypomyelination, and brain atrophy (Saitsu et al., 2010; Writzl et al., 2012; Tohyama et al., 2015). Mice and zebrafish lacking αII spectrin are embryonic and larval lethal due to cardiac and nervous system malformations (Voas et al., 2007; Stankewich et al., 2011). Many nervous system injuries and diseases including stroke and traumatic brain injury converge on spectrin degradation because spectrins are potent substrates for the Ca^{2+}-dependent protease calpain (Siman et al., 1984; Schafer et al., 2009). Therefore, breakdown of spectrins may be a common molecular pathology in neurodegenerative diseases and injuries.

βIV spectrin is enriched at AIS and nodes and forms a periodic lattice with actin (Xu et al., 2013; Leterrier et al., 2015; D'Este et al., 2017). αII spectrin is found at paranodal junctions of myelinated axons and is transiently located at developing zebrafish nodes of Ranvier (Ogawa et al., 2006; Voas et al., 2007). Although αII spectrin can coimmunoprecipitate βIV spectrin from the brain (Uemoto et al., 2007), it has not been found at AIS. Although loss of αII spectrin disrupts node formation in zebrafish (Voas et al., 2007), whether loss of spectrins is sufficient to cause axon degeneration in vertebrates remains unknown. Furthermore, because αII spectrin-deficient zebrafish and mice are larval and embryonic lethal, respectively, the postnatal functions of αII spectrin remain poorly understood. Using proteomics, biochemistry, and superresolution microscopy, we found that αII spectrin forms a periodic cytoskeleton and protein complex with βIV spectrin at AIS. To determine the function of neuronal spectrins, we generated mice lacking CNS αII spectrin. We found the αII spectrin-dependent submembranous cytoskeleton is required for many aspects of brain development and function, including assembly and maintenance of the AIS, cortical lamination, axon integrity, and proper neuronal excitability. Our results begin to reveal the many functions of the spectrin cytoskeleton in nervous system development and function.

Materials and Methods

Animals. To generate a conditional allele for *Sptan1*, a targeting vector was designed to replace an 8.5 kb genomic fragment with loxP sites flanking exon 8 of *Sptan1*. This targeting vector construct was electroporated into embryonic stem cells (ESCs) derived from 129/Sv mice. Colonies were selected and screened by Southern blot. ESCs with correct homologous recombinations were injected into blastocysts and then transferred to foster female mice. Chimeric mice were crossed with C57BL/6 mice to confirm germline transmission. Upon crossing with cre recombinase-expressing mice, exon 8 will be excised and results in the premature termination of the *Sptan1* transcript. *Sptan1*$^{f/f}$ mice were crossed with *Nestin-cre* mice to spatially eliminate αII-spectrin in the CNS. The *Sptan1*$^{f/f}$ mice were maintained on a 129/Sv and C57BL/6 mixed background. All experiments involving animals complied with National Institutes of Health (NIH) guidelines and were approved by the Animal Care and Use Committee at Baylor College of Medicine. PCR genotyping of mice was performed using the following primers: Floxed *Sptan1*: forward, 5′-AACAGTCACACCCTCTGAGTGCCA-3′; reverse, 5′-ATTCAGTGGAAAGCTGAGAAG CCAG; *Nestin-cre*: forward, 5′-TGCTGTTTCACTGGTTATGCGG-3′; reverse, 5′-TTGCCCCTGTTTC ACTATCCAG-3′.

DNA constructs. αII-spectrin-EGFP was a gift from Dr. Michael Stankewich (Yale University). The full-length βIVΣ6 spectrin with N-terminal Myc tag was provided by M. Komada (Tokyo Institute of Technology). The truncated myc-tagged βIVΣ6 spectrin was subcloned as described previously (Yang et al., 2007). The full-length βIVΣ1 spectrin with N-terminal Myc tag was subcloned and inserted into pCS3 + MT. The full-length rat 270 kDa ankG with C-terminal GFP tag (AnkG-GFP) was a gift from Dr. V. Bennett (Duke University).

Antibodies. The following primary antibodies were used: mouse monoclonal antibodies to αII-spectrin (clone D8B7, Biolegend; RRID:AB_2564660), βII-spectrin (BD Bioscience; RRID:AB_399853), αI-spectrin (clone 17C7, Abcam; RRID:AB_2194328), NeuN (EMD Millipore; RRID:AB_2298772), and Reelin (EMD Millipore; RRID:AB_2179313). The pan-NF monoclonal antibody (clone L11A/41; RRID:AB_10672370) was made by immunizing mice with a glutathione S-transferase fusion protein containing the intracellular domain of rat neurofascin. The Kv1.2 (K14/16; RRID:AB_2296313) antibodies were purchased from the University of California–Davis/NIH NeuroMab Facility. Rabbit polycolonal antibodies were as follows: βI-spectrin (Novus Biologicals; RRID:AB_11036737), βIII-spectrin (Novus Biologicals; RRID:AB_10005990), neurofilament M (EMD Millipore; RRID:AB_91201), Cux1 (Santa Cruz Biotechnology; RRID:AB_2087003), Foxp2 (Abcam; RRID:AB_2107107), Calbindin (D-28K, Swant; RRID: AB_2314111), βAPP (Thermo Fisher Scientific; RRID:AB_2533902), GFP (A-11122, Thermo Fisher Scientific; RRID:AB_221569), and βIV spectrin (generated against the peptide sequence DRAEELPRRRRP ERQE found in the C-terminal "specific domain"; RRID:AB_2315634). Rat monoclonal antibody to Ctip2 (25B6; ab18465; RRID:AB_2064130) was from Abcam. Goat polyclonal antibodies against connective tissue growth factor (ctgf, sc-14939; RRID:AB_638805) were from Santa Cruz Biotechnology. Secondary antibodies Alexa Fluor 350, 488, and 594 were from Thermo Fisher Scientific.

Immunofluorescence microscopy. Cultured neurons were fixed in 4% paraformaldehyde (PFA), pH 7.2–7.4, and immunostained as described previously (Hedstrom et al., 2008). For immunostaining of nervous system tissues, brains were collected at the indicated time points and fixed in 4% PFA on ice for 1 h. Brains were then immersed in 20% sucrose in 0.1 M PB overnight at 4°C and then embedded in optimal cutting temperature compound (Tissue-Tek; #4583) and sectioned using a cryostat (Thermo Fisher Scientific; Cryostar NX70) on glass coverslips for immunostaining. Procedures for immunofluorescence labeling were performed as described previously (Ogawa et al., 2006). Images of immunofluorescence were captured using an Axio-imager Z1 microscope (Carl Zeiss) or Axio-observer Z1 microscope (Carl Zeiss) fitted with an AxioCam digital camera (Carl Zeiss). Images were taken using 20×/0.8 numerical aperture (NA), 40×/1.0 NA, 40×/0.75 NA, or 63×/1.4 NA objectives. Images were then collected by Zen (Carl Zeiss) acquisition software. Measurement of fluorescence intensity and Sholl analysis was performed using FIJI and Zen software. In some cases, *Z*-stacks and 3D reconstructions were performed using Zen software.

Superresolution Stochastic Optical Reconstruction Microscopy (STORM) and DNA-PAINT. Twelve days *in vitro* (DIV) neurons were fixed using 4% PFA for 10 min. After blocking, they were incubated with primary antibodies overnight at 4°C, then with secondary antibodies for 1 h at room temperature. STORM imaging was performed on an N-STORM microscope (Nikon Instruments). Coverslips were imaged in STORM buffer containing the following: 50 mM Tris, pH 8, 10 mM NaCl, 10% glucose, 100 mM MEA, 3.5 U/ml pyranose oxidase, and 40 mg/ml catalase. The sample was illuminated continuously at 647 nm (full power) and 30,000–60,000 images were acquired at 67 Hz, with progressive reactivation by simultaneous 405 nm illumination (Leterrier et al., 2015). For DNA-PAINT labeling, fixed coverslips were incubated with primary antibodies and then with DNA-conjugated secondary antibodies (Ultivue) for 1 h at room temperature. Samples were imaged in imaging buffer with 0.32 nM Imager-650 and 0.16 nM Imager-560 (Ultivue). The sample was alternatively illuminated at 647 and 561 nm (full laser power) and 20,000–30,000 images of each channel were acquired at 25–33 Hz.

Immunoprecipitation and immunoblotting. COS-7 cells were transfected with αII-spectrin-EGFP along with different Myc-tagged βIV-spectrin Σ1, Σ6, and truncated plasmids (Yang et al., 2007). For a negative control, cells were transfected with GFP along with βIV-spectrin Σ1 or βIV-spectrin Σ6. Two days after transfection, cells were collected and lysed with 250 μl of lysis buffer (20 mM Tris-HCl, pH 8.0, 10 mM EDTA, pH 8.0, 150 mM NaCl) containing 1% Triton X-100 and protease inhibitors at 4°C for 1 h with agitation. Cell lysates were then centrifuged at 13,000 × *g* at 4°C for 10 min. The soluble supernatants were incubated overnight with GFP antibody-coupled protein A or G agarose beads (GE Healthcare). The beads were washed 7 times with 1 ml of lysis buffer and

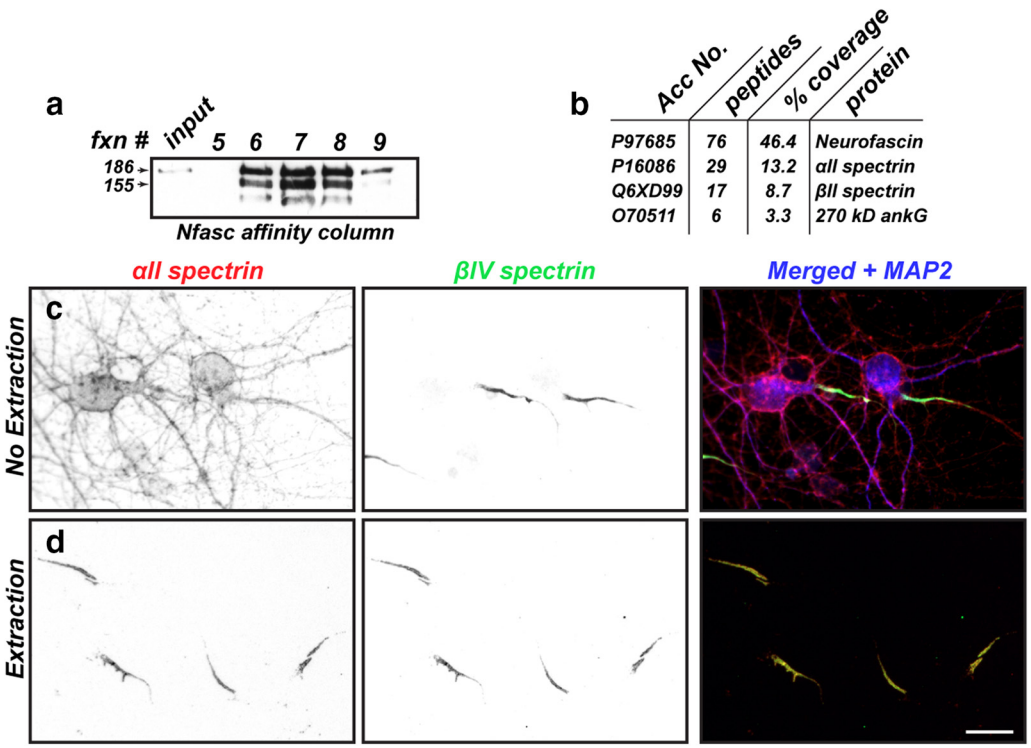

Figure 1. αII spectrin is found at the AIS. ***a***, Immunoblot of neurofascin (Nfasc) purified from rat brain using an anti-Nfasc affinity column. Fractions 5–9 are shown. ***b***, Proteins purified from the Nfasc affinity column identified by mass spectrometry. ***c***, Immunostaining of 12 DIV rat hippocampal neurons using antibodies against αII spectrin (red), βIV spectrin (green), and MAP2 (blue). ***d***, Detergent-extracted 12 DIV rat hippocampal neurons immunostained using antibodies against αII spectrin (red), βIV spectrin (green), and MAP2 (blue). Scale bar, 20 μm.

then eluted with 20 μl of 2× reducing sample buffer at 100°C for 5 min. The immunoprecipitates and the total supernatant as input were separated by SDS-PAGE, transferred to nitrocellulose membrane (GE Healthcare), and detected by immunoblotting using Myc or GFP antibody.

Neurofascin affinity purification. The neurofascin affinity column was made by coupling mouse monoclonal antibodies to neurofascin (clone A12/18.1, RRID:AB_2282826) using the Affi-Gel Hz Immunoaffinity kit (Bio-Rad) according to the manufacturer's instructions. Rat brain membrane homogenates were solubilized using RIPA buffer (1% Triton X-100, 1% sodium deoxycholate, 0.1% SDS, 0.15 M NaCl, 20 mM HEPES, 10 mM EDTA, pH 8.0, and protease inhibitors) at 4°C. The detergent-soluble fraction was then run over the affinity column three times. The column was washed with 50 ml of RIPA buffer, followed by elution of bound proteins using 10 ml of 0.1 M glycine, pH 2.5. Eluted proteins were collected in 1 ml fractions containing 100 μl of 1 M Tris, pH 8.7. The proteins in each fraction were then precipitated by ethanol precipitation.

Reverse-phase LC-MS/MS analysis. Purified proteins were size fractionated by SDS PAGE and protein bands were excised. Purified proteins were then identified using mass spectrometry as described previously (Ogawa et al., 2010).

In utero *electroporation. In utero* electroporation was performed as described previously (Hedstrom et al., 2007). GFP and αII spectrin shRNA plasmids (Galiano et al., 2012) were introduced into rat embryos at embryonic day 16 (E16). After recovery of the mother, newborn pups were killed at postnatal day 7 (P7) for immunostaining.

EEG. Mice were implanted with bilateral silver wire cortical EEG electrodes under Avertin anesthesia as described previously (Olivetti et al., 2014). Recordings were obtained after recovery with 8 h monitoring periods for 1 week after recovery using a Stellate Systems Harmonie 10 video EEG system. EEGs were analyzed by two observers blinded to genotype.

Hippocampal neurons. Primary cultures of hippocampal neurons were obtained from E18.5 Sprague Dawley rat embryos or P1–P2 mouse neonates. Hippocampi were dissected and dissociated. Neurons were then plated onto poly-D-lysine- and laminin-coated glass coverslips. Hippocampal neurons were cultured in Neurobasal medium (Life Technologies) containing 1% Glutamax (Life Technologies), 1% penicillin/streptomycin (Life Technologies), and 2% B27 supplement (Life Technologies) in a 5% CO_2 incubator. For detergent extraction studies, hippocampal neurons and teased nerves were incubated with ice-cold PBS containing 0.5% Triton X-100 at 4°C for 30 min or 1 h, respectively. Neurons or nerves were then washed with 1× PBS 3 times and then processed using the regular immunofluorescence procedures. In some cases, we infected hippocampal neurons using AAV-cre-GFP virus (AAV-EF1α-EGFP-T2A-iCre (serotype: AAV-DJ8)) or adenovirus to express control shRNA or αII spectrin shRNA. The AAV virus was obtained from the Intellectual and Developmental Disabilities Research Center Neuroconnectivity Core at Baylor College of Medicine and produced by Dr. B. Arenkiel (Baylor College of Medicine); the adenovirus was as described previously (Galiano et al., 2012).

Statistics. No statistical methods were used to predetermine sample sizes, but our sample sizes are similar to those reported previously (Susuki et al., 2013). All statistical analyses were performed using GraphPad Prism software or Microsoft Excel. Error bars in figures are ± SEM. Unpaired, two-tailed Student's *t* test was used for statistical analyses unless otherwise specified. Except for EEG, data collection and analyses were not performed blinded to the conditions of the experiments. Data distribution was assumed to be normal.

Results

αII spectrin forms a periodic cytoskeleton with βIV spectrin at the AIS

AIS have two main functions: to initiate action potentials and to regulate neuronal polarity. These properties require the ankG-dependent AIS cytoskeleton (Hedstrom et al., 2008; Kole et al., 2008). However, apart from ankG and βIV spectrin, the composition of the AIS cytoskeleton remains poorly understood. To identify new AIS proteins that may contribute to AIS structure and function, we made an anti-neurofascin antibody-conjugated affinity column to purify NF186 and its associated proteins from rat brain homogenate; NF186 is an ankyrin-binding cell adhesion molecule clustered at the AIS. Immunoblots of fractions eluted

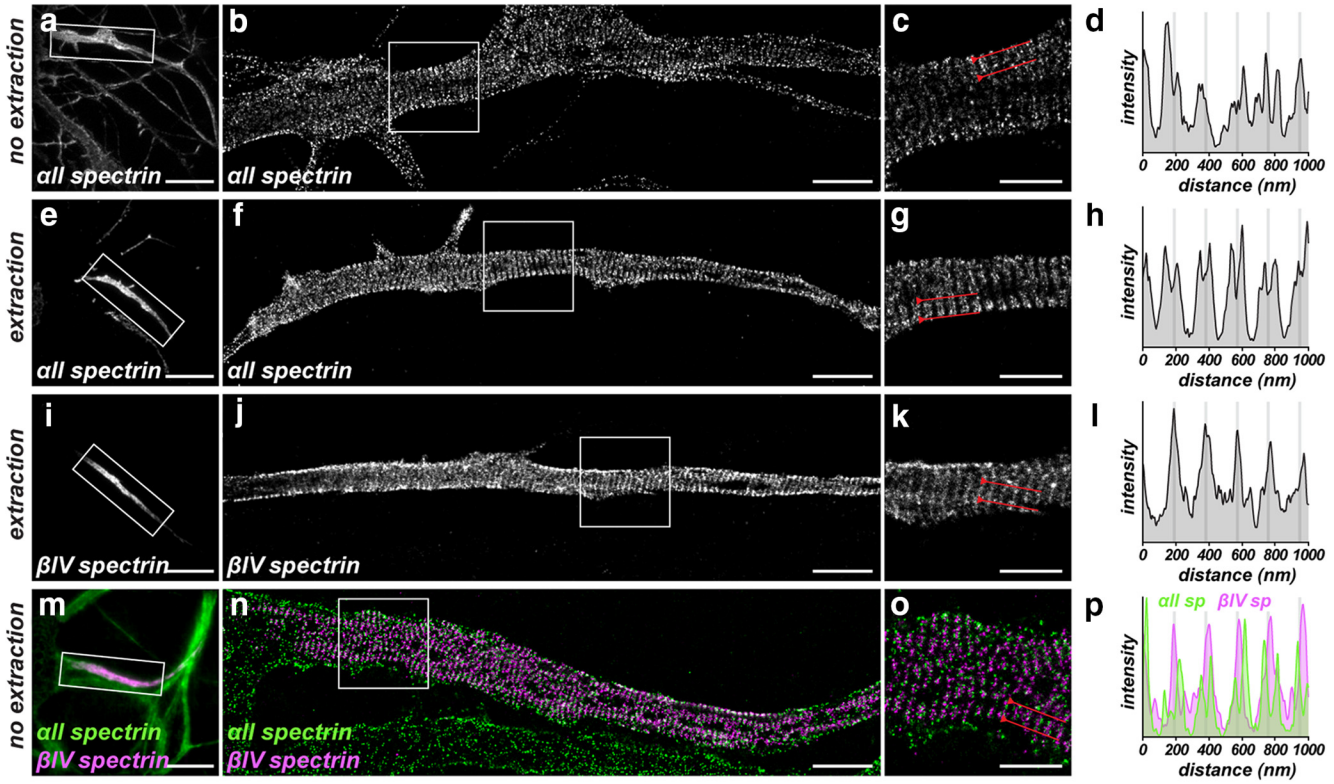

Figure 2. αII spectrin forms a periodic cytoskeleton with βIV spectrin at AIS. ***a–d***, Conventional fluorescence (***a***) and STORM (***b***, ***c***) imaging of 12 DIV cultured hippocampal neurons labeled with antibodies against αII spectrin. The box in ***a*** corresponds to the STORM image shown in ***b***. The box in ***b*** corresponds to the STORM image shown in ***c***. The region between the lines in ***c*** was used to generate an αII spectrin intensity profile ***d***. Scale bars: ***a***, 10 μm; ***b***, 2 μm; ***c***, 1 μm. ***e–h***, Conventional fluorescence (***e***) and STORM (***f***, ***g***) imaging of detergent-extracted 12 DIV cultured hippocampal neurons labeled with antibodies against αII spectrin. The box in ***e*** corresponds to the STORM image shown in ***f***. The box in ***f*** corresponds to the STORM image shown in ***g***. The region between the lines in ***g*** was used to generate an αII spectrin intensity profile (***h***). Scale bars: ***e***, 10 μm; ***f***, 2 μm; ***g***, 1 μm. ***i–l***, Conventional fluorescence (***i***) and STORM (***j***, ***k***) imaging of detergent-extracted 12 DIV cultured hippocampal neurons labeled with antibodies against βIV spectrin. The box in ***i*** corresponds to the STORM image shown in ***j***. The box in ***j*** corresponds to the STORM image shown in ***k***. The region between the lines in ***k*** was used to generate a βIV spectrin intensity profile (***l***). Scale bars: ***i***, 10 μm; ***j***, 2 μm; ***k***, 1 μm. ***m–p***, Conventional fluorescence (***m***) obtained by projecting frames from the PAINT acquisition sequence and DNA-PAINT (***n***, ***o***) imaging of 12 DIV cultured hippocampal neurons labeled with antibodies against αII spectrin and βIV spectrin. The box in ***m*** corresponds to the PAINT image shown in ***n***. The box in ***n*** corresponds to the PAINT image shown in ***o***. The region between the lines in ***o*** was used to generate αII spectrin (green) and βIV spectrin (magenta) intensity profiles (***p***). Scale bars: ***m***, 10 μm; ***n***, 2 μm; ***o***, 1 μm.

from this affinity column showed a strong chromatographic peak for both neuronal NF186 and oligodendroglial NF155 (Fig. 1*a*). We pooled fractions 6–8, precipitated the proteins, and then size fractionated them by SDS-PAGE. We excised proteins from the gels and then performed mass spectrometry and found, as expected, that the most abundant protein purified was neurofascin (Fig. 1*b*). The next most abundant protein was αII spectrin. αII spectrin attracted our attention because βIV spectrin is highly enriched at the AIS (Fig. 1*c*) and can form a complex with αII spectrin (Uemoto et al., 2007). However, αII spectrin has not been reported at the AIS. Consistent with our previous study (Galiano et al., 2012), immunostaining of αII spectrin in 12 DIV rat hippocampal neurons revealed widespread and diffuse labeling rather than specific enrichment at the AIS (Fig. 1*c*). Remarkably, detergent extraction of 12 DIV neurons before fixation revealed a pool of detergent-resistant αII spectrin only at the AIS that also colocalized with βIV spectrin (Fig. 1*d*).

To define the precise distribution of αII spectrin in the AIS, we used STORM (Rust et al., 2006). STORM imaging of nondetergent extracted and αII spectrin-labeled AIS revealed a periodic organization like that previously reported for ankG, βIV spectrin, Na^+ channels, and NF186 (Fig. 2*a–d*; Xu et al., 2013; Zhong et al., 2014; Leterrier et al., 2015). However, detergent extraction showed an even clearer periodicity (Fig. 2*e–h*) with two resolvable peaks of immunofluorescence very close to one another (Fig. 2*g*,*h*). In contrast, STORM imaging of detergent-extracted AIS using antibodies against the C terminus of βIV spectrin showed only one major peak with a periodicity of ~190 nm (Fig. 2*i–l*). To visualize αII spectrin and βIV spectrin simultaneously, we combined DNA-PAINT labeling (Jungmann et al., 2014) with STORM imaging (Fig. 2*m–p*). Intensity profiles revealed that the two peaks of αII spectrin immunoreactivity flank βIV spectrin labeling (Fig. 2*p*). The labeling patterns are consistent with a model in which spectrin tetramers space actin rings because the αII spectrin antibodies were generated against the SH3 domain located after spectrin repeat (SR) 9, resulting in two resolvable peaks of fluorescence intensity surrounding the single peak resulting from labeling of the C terminus of βIV spectrin. Furthermore, these two-color DNA-PAINT images demonstrate directly *in situ* that α spectrins are arranged head-to-head in the spectrin tetramer. Therefore, αII spectrin is found at the AIS, where it forms a periodic cytoskeleton with βIV spectrin.

αII spectrin interacts with βIV spectrin splice variants

How do αII and βIV spectrin interact? Alternative splicing generates up to six βIV spectrin splice variants (Berghs et al., 2000). Among these, βIVΣ1 and βIVΣ6 are at AIS and nodes of Ranvier (Komada and Soriano, 2002; Lacas-Gervais et al., 2004; Yoshimura et al., 2016). βIVΣ1 is the longest splice variant and includes an N-terminal actin-binding domain, 17 SRs, a "spe-

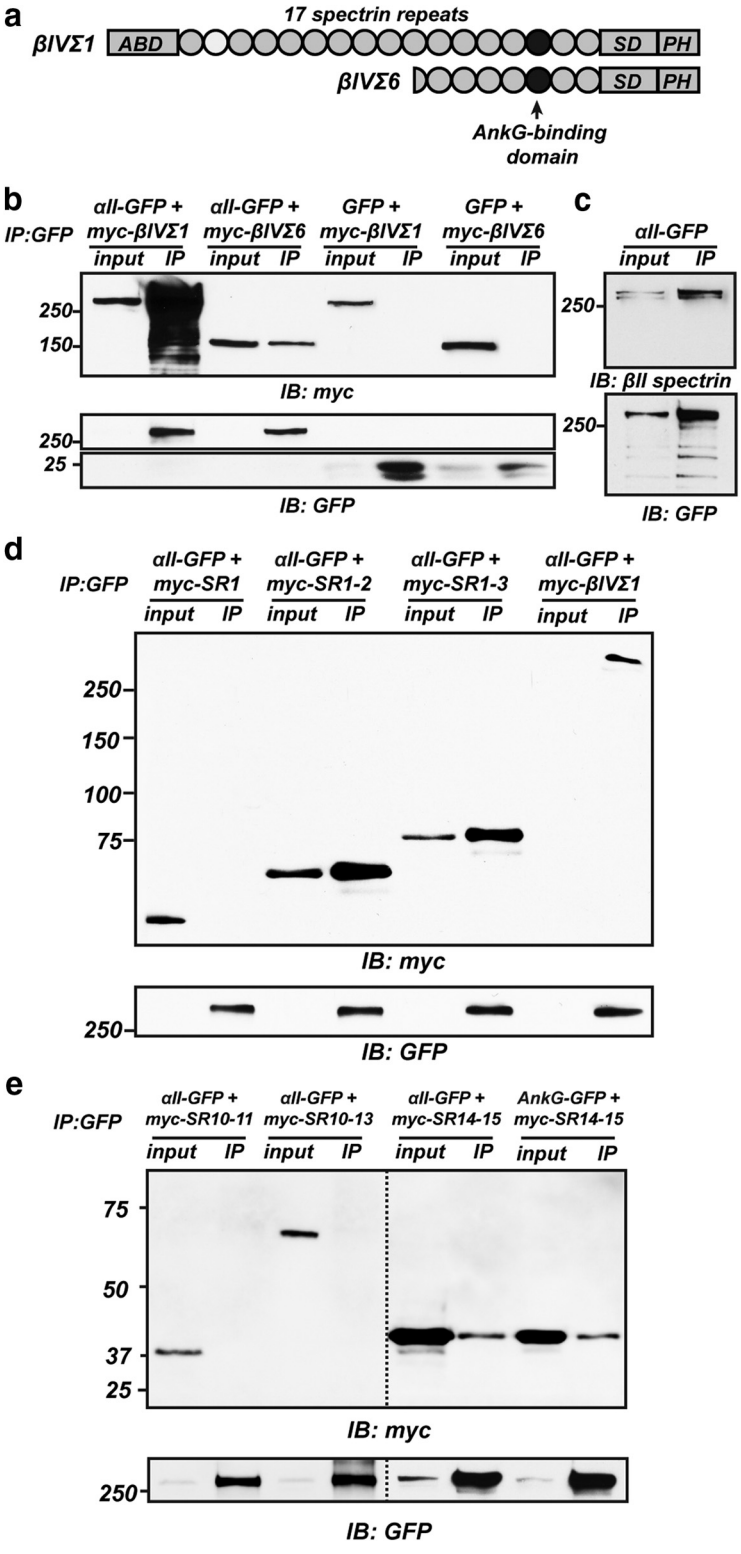

Figure 3. αII spectrin and βIV spectrin splice variants can interact through SR1-2 and SR14-15. ***a***, Diagram of βIV spectrin splice variants and their domains. ABD, actin-binding domain; SD, specific domain; PH, pleckstrin homology domain. ***b***, Cotransfection of COS-7 cells with GFP-tagged αII spectrin and myc-tagged βIVΣ1 or βIVΣ6. Immunoprecipitation of αII spectrin-GFP coimmunoprecipitates both myc-βIVΣ1 and myc-βIVΣ6. Immunoblots were performed using antibodies against myc and GFP. Molecular weights are shown in kDa. ***c***, Transfection of GFP-tagged αII spectrin in COS-7 cells. Immunoprecipitation of αII spectrin-GFP coimmunoprecipitates endogenous βII spectrin. ***d***, Cotransfection of COS-7 cells with GFP-tagged αII spectrin and myc-tagged SR1, SR1-2, or SR1-3. Immunoprecipitation using anti-GFP antibodies coimmunoprecipitates myc-SR1-2 and myc-SR1-3. Molecular weights are shown in kilodaltons (kDa). Coimmunoprecipitation between αII spectrin-GFP and myc-βIVΣ1 is included as a positive control. ***e***, Cotransfection of COS-7 cells with αII spectrin-GFP and myc-tagged SR10-11, SR10-13 or SR14-15. αII spectrin-GFP coimmunoprecipitates myc-SR14-15. Molecular weights are shown in kilodaltons (kDa). Coimmunoprecipitation between AnkG-GFP and myc-SR14-15 is included as a positive control.

cific" domain (SD), and a C-terminal pleckstrin homology domain. In contrast, βIVΣ6 is an N-terminal truncation lacking the actin-binding domain and the first 9 SRs (Fig. 3*a*). Although βIVΣ1 and βIVΣ6 are both expressed throughout brain development, βIVΣ6 is expressed at the highest levels and is the major splice variant at mature AIS and nodes of Ranvier (Yoshimura et al., 2016). αII spectrin was shown previously to coimmunoprecipitate both βIVΣ1 and βIVΣ6 from the brain (Uemoto et al., 2007). To confirm that αII spectrin can interact with βIV spectrin splice variants, we cotransfected αII spectrin-GFP (αII-GFP) and myc-βIV spectrins (myc-βIVΣ1 or myc-βIVΣ6) into COS-7 cells. Immunoprecipitation using antibodies against GFP confirmed that αII spectrin binds to both βIVΣ1 and βIVΣ6 (Fig. 3*b*), but βIVΣ1 bound to αII spectrin much more strongly than βIVΣ6 and neither interacted with GFP alone. Endogenous βII spectrin was also detected in COS-7 cells and could be coimmunoprecipitated with αII-GFP (Fig. 3*c*). αII spectrin's ability to bind both βIVΣ1 and βIVΣ6 is surprising because α and β spectrins are thought to interact through β spectrin's first two SRs (Speicher et al., 1992). To determine how αII spectrin and βIV spectrin splice variants interact, we constructed different truncated myc-tagged βIV spectrin proteins consisting of SR1, SR1-2, SR1-3, SR10-11, SR10-13, and SR14-15 and cotransfected these with αII-GFP (Fig. 3*d*,*e*). Consistent with previous models for α and β spectrin interactions (Speicher et al., 1992), we found that SR1-2 strongly bound αII spectrin (Fig. 3*d*). However, these experiments also revealed a second, lower-affinity binding site (SR14-15) found in both βIVΣ1 and βIVΣ6 splice variants (Fig. 3*e*). Intriguingly, SR14-15 is also the binding site for ankG and is required for βIV spectrin recruitment to AIS and nodes (Yang et al., 2007). Therefore, βIVΣ1 binds strongly to αII spectrin through two distinct SRs and βIVΣ6, despite lacking the N-terminal SR1-2, can also interact with αII spectrin through SR14-15.

Loss of αII spectrin causes widespread CNS abnormalities

Constitutive knock-out of αII spectrin causes embryonic lethality in mice (Stankewich et al., 2011) and larval lethality in zebrafish (Voas et al., 2007). To determine the function of αII spectrin in the postnatal brain, we generated αII spectrin floxed mice (*Sptan1*$^{f/f}$) and crossed them with *Nestin-cre* mice to eliminate αII spectrin

selectively in the CNS. We introduced *LoxP* sites flanking exon 8 of *Sptan1*. Upon recombination by Cre recombinase, exon 8 is excised, resulting in a frameshift mutation and premature stop codon near the end of SR3. We confirmed loss of αII spectrin protein by immunostaining of cerebellar sections (Fig. 4*a*); αII spectrin was detected only in endothelial cells in *Nestin-cre;Sptan1*$^{f/f}$ brains. To further confirm loss of αII spectrin protein and to examine the consequence for β spectrins, we performed immunoblots on brain homogenates (Fig. 4*b*). As expected, αII spectrin protein was nearly undetectable. Furthermore, we did not detect any αI spectrin in either control or *Nestin-cre;Sptan1*$^{f/f}$ mice, consistent with the conclusion that there is no compensation by αI spectrin and αII spectrin is the main α spectrin detected in the brain (Zhang et al., 2014). Importantly, we measured a profound reduction in the amount of all β spectrins (with the exception of βIVΣ6, which was increased 4.5-fold; Fig. 4*b*). *Nestin-cre;Sptan1*$^{f/f}$ mice were smaller than their littermate controls and loss of αII spectrin resulted in juvenile lethality (Fig. 4*c*). *Nestin-cre;Sptan1*$^{f/f}$ mice also had smaller brains with enlarged ventricles (data not shown). Therefore, loss of αII spectrin disrupts spectrin cytoskeletons throughout the CNS, making the *Sptan1*$^{f/f}$ mice a powerful tool with which to study the importance of submembranous spectrin cytoskeletons in nervous system function.

Because αII spectrin forms a complex with βIV spectrin at the AIS, we examined AIS in the cortex of *Nestin-cre;Sptan1*$^{f/f}$ mice and found that, compared with controls, there were far fewer AIS and those present were fragmented and disrupted (Fig. 5*a*). We measured a reduction in the number of βIV spectrin-labeled AIS/1000 μm^2 from 30.2 ± 2.8 μm in *Sptan1*$^{f/f}$ cortex to 2.85 ± 0.28 in *Nestin-cre;Sptan1*$^{f/f}$ cortex ($n = 3$ for each genotype, $p = 0.0006$, $t = 9.916$, df = 4). The reduction in βIV spectrin-labeled AIS occurred despite the increased expression of the βIVΣ6 splice variant (Fig. 4*b*). This is consistent with the fact that βIVΣ6 alone is not sufficient to rescue AIS properties (Lacas-Gervais et al., 2004). To examine the consequence of loss of αII spectrin on the organization of the AIS and axonal cytoskeletons, we performed STORM imaging on cultured *Sptan1*$^{f/f}$ hippocampal neurons transduced with AAV-Cre-GFP. STORM imaging showed that, whereas control (GFP^-) neurons had intact βIV spectrin staining and periodicity at the AIS (Fig. 5*b–e*), neurons lacking αII spectrin (GFP^+) had significantly less clustered βIV spectrin and the periodicity was disrupted dramatically (Fig. 5*f–i*). αII spectrin interacts with βII spectrin in the distal axon (Galiano et al., 2012) and βII spectrin forms a periodic cytoskeleton there (Fig. 5*j–m*) (Xu et al., 2013).

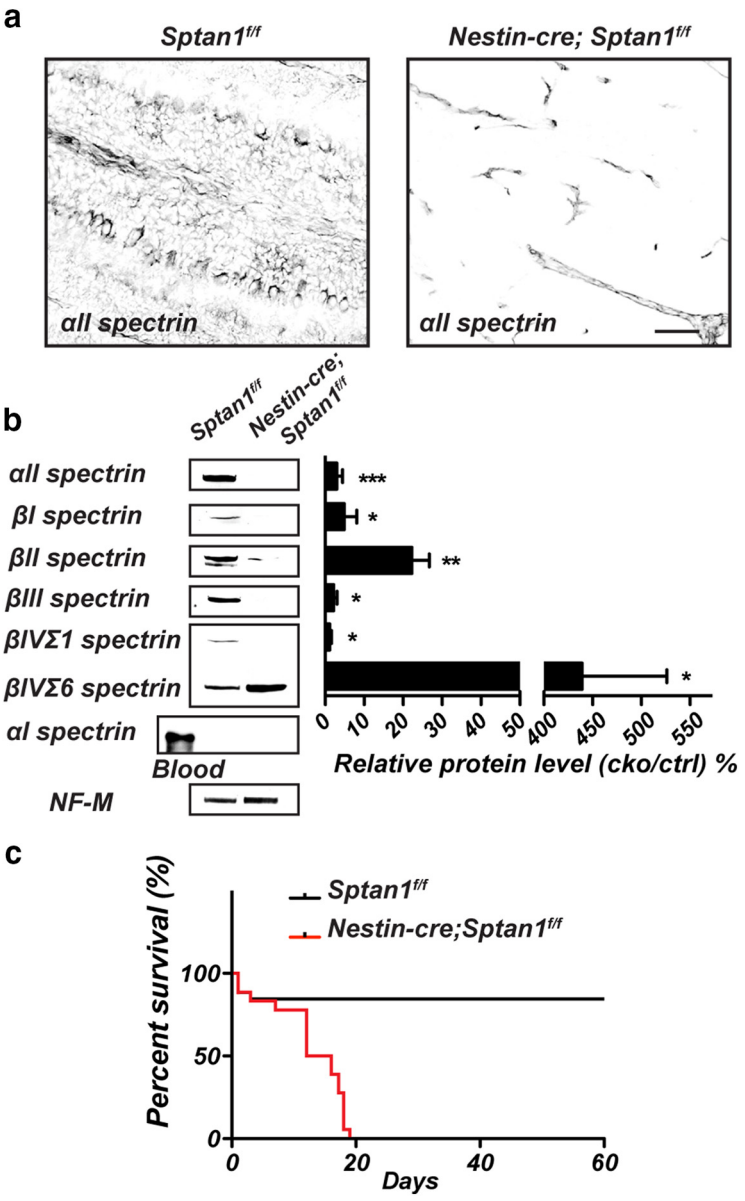

Figure 4. Mice lacking nervous system αII spectrin. ***a***, αII spectrin immunostaining in cerebella of P12 *Sptan1*$^{f/f}$ and *Nestin-cre;Sptan1*$^{f/f}$ mice. ***b***, Immunoblots of brain membrane homogenates from P7 *Sptan1*$^{f/f}$ and *Nestin-cre;Sptan1*$^{f/f}$ mice using antibodies against the indicated spectrins. Blood was used as the positive control for αI spectrin. Neurofilament-M (NF-M) served as the loading control. Protein levels were calculated as the percentage of *Nestin-cre;Sptan1*$^{f/f}$ mice compared with *Sptan1*$^{f/f}$ mice. $n = 3$ mice per genotype. Mean ± SEM αII: $p = 0.0009$; βI: $p = 0.0234$; βII: $p = 0.0042$; βIII: $p = 0.032$; βIV-Σ1: $p = 0.0112$; βIV-Σ6: $p = 0.0174$. αII: $t_{(4)} = 21.47$; βI: $t_{(4)} = 3.57$; βII: $t_{(4)} = 5.89$; βIII: $t_{(4)} = 3.228$; βIV-Σ1: $t_{(4)} = 4.46$; βIV-Σ6: $t_{(4)} = 3.912$. ***c***, Survival curve for *Sptan1*$^{f/f}$ ($n = 26$) and *Nestin-cre;Sptan1*$^{f/f}$ mice ($n = 18$). *$p < 0.05$; **$p < 0.01$; ***$p < 0.001$.

Similar to the AIS, loss of αII spectrin disrupted the periodicity of the βII spectrin-containing distal axon cytoskeleton (Fig. 5*n–q*). Therefore, loss of αII spectrin affects multiple β spectrins and has widespread effects on the organization of the axonal cytoskeleton.

Human mutations in *SPTAN1* cause severe epilepsy (Saitsu et al., 2010). The *Nestin-cre;Sptan1*$^{f/f}$ mice recapitulated this phenotype with generalized seizures lasting from 3 to 20 s and involving nearly continuous fine limb movements. EEG recordings (Fig. 6*a*) revealed spike frequencies of 0.25 ± 0.1 ($n = 4$, ±SEM) and 40.3 ± 17.0 ($n = 5$, ±SEM) spikes/h in control and *Nestin-cre;Sptan1*$^{f/f}$ mice, respectively ($p = 0.0159$, Fig. 6*b*); control mice displayed no abnormal EEG discharges.

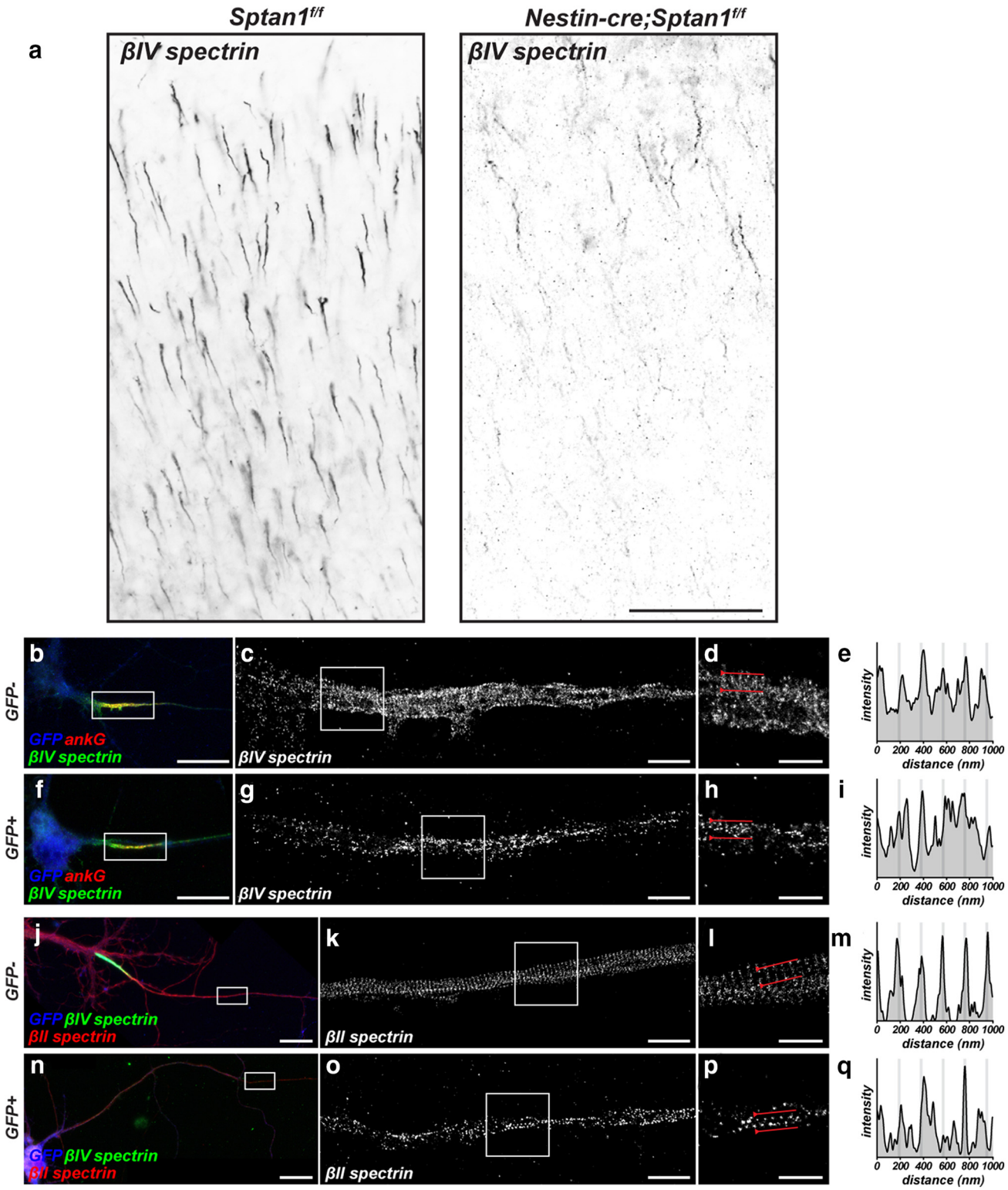

Figure 5. Loss of αII spectrin disrupts the AIS cytoskeleton. ***a***, AIS immunostained for βIV spectrin in P18 *Sptan1* $^{f/f}$ and *Nestin-cre;Sptan1* $^{f/f}$ cerebral cortex. Scale bar, 20 μm. ***b***–***e***, Conventional fluorescence (***b***) and STORM (***c***, ***d***) imaging of GFP $^{-}$ 12 DIV cultured hippocampal neurons labeled with antibodies against GFP (blue), ankG (red), and βIV spectrin (green). The box in ***b*** corresponds to the STORM image shown in ***c***. The box in ***c*** corresponds to the STORM image shown in ***d***. The region between the lines in ***d*** was used to generate a βIV spectrin intensity profile (***e***). Scale bars: ***b***, 10 μm; ***c***, 2 μm; ***d***, 1 μm. ***f***–***i***, Conventional fluorescence (***f***) and STORM (***g***, ***h***) imaging of GFP $^{+}$ 12 DIV cultured hippocampal neurons labeled with antibodies against GFP (blue), ankG (red), and βIV spectrin (green). The box in ***f*** corresponds to the STORM image shown in ***g***. The box in ***g*** corresponds to the STORM image shown in ***h***. The region between the lines in ***h*** was used to generate a βIV spectrin intensity profile (***i***). Scale bars: ***f***, 10 μm; ***g***, 2 μm; ***h***, 1 μm. ***j***–***m***, Conventional fluorescence (***j***) and STORM (***k***, ***l***) imaging of GFP $^{-}$ 12 DIV cultured hippocampal neurons labeled with antibodies against GFP (blue), βII spectrin (red), and βIV spectrin (green). The box in ***j*** corresponds to the STORM image shown in ***k***. The box in ***k*** corresponds to the STORM image shown in ***l***. The region between the lines in ***l*** was used to generate a βII spectrin intensity profile (***m***). Scale bars: ***j***, 10 μm; ***k***, 2 μm; ***l***, 1 μm. ***n***–***q***, Conventional fluorescence (***n***) and STORM (***o***, ***p***) imaging of GFP $^{+}$ 12 DIV cultured hippocampal neurons labeled with antibodies against GFP (blue), βII spectrin (red), and βIV spectrin (green). The box in ***n*** corresponds to the STORM image shown in ***o***. The box in ***o*** corresponds to the STORM image shown in ***p***. The region between the lines in ***p*** was used to generate a βII spectrin intensity profile (***q***). Scale bars: ***n***, 10 μm; ***o***, 2 μm; ***p***, 1 μm.

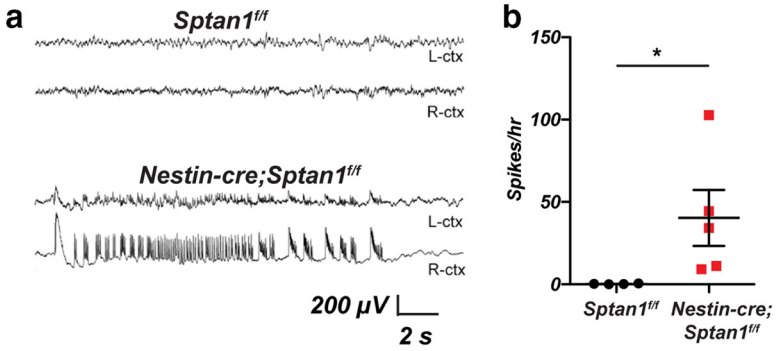

Figure 6. αII spectrin-deficient mice have seizures. ***a***, Video EEG monitoring of awake and behaving P12–P14 mice revealed generalized seizure discharges in *Nestin-cre;Sptan1*$^{f/f}$ mice that were not detected in *Sptan1*$^{f/f}$ littermates. ***b***, Quantification of spikes/h recorded in *Sptan1*$^{f/f}$ and *Nestin-cre;Sptan1*$^{f/f}$ mice. *$p = 0.0159$.

In addition to intrinsic axonal excitability changes arising from AIS disruption, epilepsy may also result from cortical malformations and aberrant neuronal layering (Guerrini and Dobyns, 2014). Immunostaining of *Nestin-cre;Sptan1*$^{f/f}$ cortex with antibodies against neurons normally restricted to distinct cortical layers revealed disrupted cortical lamination. We found that, at both P7 and P12, Reelin$^+$, Ctip2$^+$, Foxp2$^+$, and ctgf$^+$ neurons corresponding to distinct cortical layers were frequently dispersed among other layers (Fig. 7*a*,*b*). For example, at P12, many Ctip2-labeled neurons (layer V) were found in layers II–IV (Cux1$^+$ region), whereas Reelin$^+$ neurons were distributed more broadly throughout the cortex at both P7 and P12 (Fig. 7*c*,*d*).

To gain insight into the causes of disrupted cortical lamination, we performed *in utero* electroporation to label migrating neurons and to silence expression of αII spectrin using a highly efficient short hairpin RNA (shRNA) (Galiano et al., 2012). This allowed us to examine the cell-autonomous consequence of loss of αII spectrin during development in single neurons. We found that, in contrast to electroporation with GFP alone (Fig. 7*e*), at P7, electroporated neurons lacking αII spectrin were frequently arrested in their migration through the cortical plate. αII spectrin-deficient neurons also lacked dendrites and remained in a migrating bipolar morphology (Fig. 7*f*). To examine more directly the effect of loss of αII spectrin on dendrite morphology, we transduced cultured rat hippocampal neurons at 1 DIV using adenovirus to express a control shRNA or αII spectrin shRNA (Galiano et al., 2012). At 17 DIV, we measured the extent of dendritic arborization and found a reduced complexity ($n = 3$ independent experiments for each condition; Fig. 7*g*). Therefore, loss of αII spectrin causes severe epilepsy that may reflect disrupted AIS, reduced dendritic complexity, and abnormal development of neural circuits due to impaired neuronal migration.

Consistent with widespread abnormalities in brain organization, when we examined the cerebellum, we found significantly fewer Purkinje neurons (53.3 ± 1.3 cells/mm and 29.3 ± 0.8 cells/mm in WT and *Nestin-cre;Sptan1*$^{f/f}$ mice, respectively; $p = 0.0001$, $t_{(4)} = 2.5$) and the *Nestin-cre;Sptan1*$^{f/f}$ Purkinje neuron AIS were fragmented and much shorter than those in control *Sptan1*$^{f/f}$ mice (Fig. 7*h*,*i*). Cerebellar pinceaux, labeled for Kv1.2 and corresponding to basket cell terminals, were also disrupted in αII spectrin-deficient cerebellum (Fig. 7*h*). Furthermore, control AIS were usually oriented ±30° perpendicular to the plane of the Purkinje neuron layer, but *Nestin-cre;Sptan1*$^{f/f}$ mice had AIS that deviated much further from the perpendicular axis (Fig. 7*h*,*i*), indicating that altered axonal projections may also contribute to circuit dysfunction in αII spectrin-deficient mice. Finally, the molecular layer at P18 was also significantly thinner in *Nestin-cre;Sptan1*$^{f/f}$ mice (97.3 ± 4.8 μm in *Sptan1*$^{f/f}$ mice and 70.0 ± 3.3 μm in *Nestin-cre;Sptan1*$^{f/f}$ mice; $n = 3$ for each genotype, $p = 0.006$, $t = 5.15$, df = 4).

What accounts for the reduced numbers of Purkinje neurons, thinner molecular layer, and disrupted brain organization? Because neuronal cytoskeletons are thought to play important roles in neurons, one possibility is that αII spectrin-deficient neurons may degenerate. To test this, we immunostained brain sections using antibodies against beta-amyloid precursor protein (β-APP), a robust marker of axonal injury and degeneration (Gentleman et al., 1993). We found widespread immunostaining for β-APP in *Nestin-cre;Sptan1*$^{f/f}$ Purkinje neurons in the cerebellum and throughout the thalamus and cortex (Fig. 8*a*–*c*). These results show that loss of αII spectrin leads to widespread CNS neurodegeneration.

Discussion

Submembranous spectrin cytoskeletons are found in all eukaryotic cells and are thought to confer both flexibility and strength to cell membranes and to participate in organizing and maintaining the distribution of membrane proteins. These conclusions are based on detailed studies of erythrocyte spectrins and human αI spectrin mutations that cause spherocytic anemia due to a fragile cell membrane (Perrotta et al., 2008). However, much less is known about spectrins in the nervous system. Although human mutations in αII spectrin cause severe epilepsy (Saitsu et al., 2010; Tohyama et al., 2015), previous studies of spectrin function have mostly focused on the role of β spectrins. For example, human mutations in βIII spectrin cause spinocerebellar ataxia type 5 (Ikeda et al., 2006) and mouse and human mutations in βIV spectrin cause deafness, neuropathy, and ataxia (Parkinson et al., 2001; Komada and Soriano, 2002; Yang et al., 2004; Knierim et al., 2017). Determining the function of the spectrin cytoskeleton in vertebrates has been complicated by the diversity of β spectrins and by the fact β spectrins may compensate for one another (Ho et al., 2014). The function of αII spectrin has been studied in mice and zebrafish, but animals lacking αII spectrin die at the embryonic and larval stages, respectively (Voas et al., 2007; Stankewich et al., 2011), precluding any studies of physiology or behavior or determination of the role of αII spectrin in maintenance of neuronal integrity and function.

Here, we confirmed that αII spectrin is the major α spectrin found in the brain and is required for proper expression of all other β spectrins. Therefore, our αII spectrin conditional knockout mouse represents an attractive model to study, not only West syndrome, a severe form of infantile spasms for which only one other nonlethal genetic mouse model has been reported (Olivetti et al., 2014), but more broadly the function of the neuronal spectrin-based submembranous cytoskeleton. We demonstrate that αII spectrin plays diverse roles in the nervous system including, but not limited to, AIS assembly, neuronal migration, excitability, and health. These pleiotropic functions of αII spectrin likely reflect different roles depending on the cell type and which of the neuronal β spectrins it is partnered with. Future experiments will be required to further define the contributions of

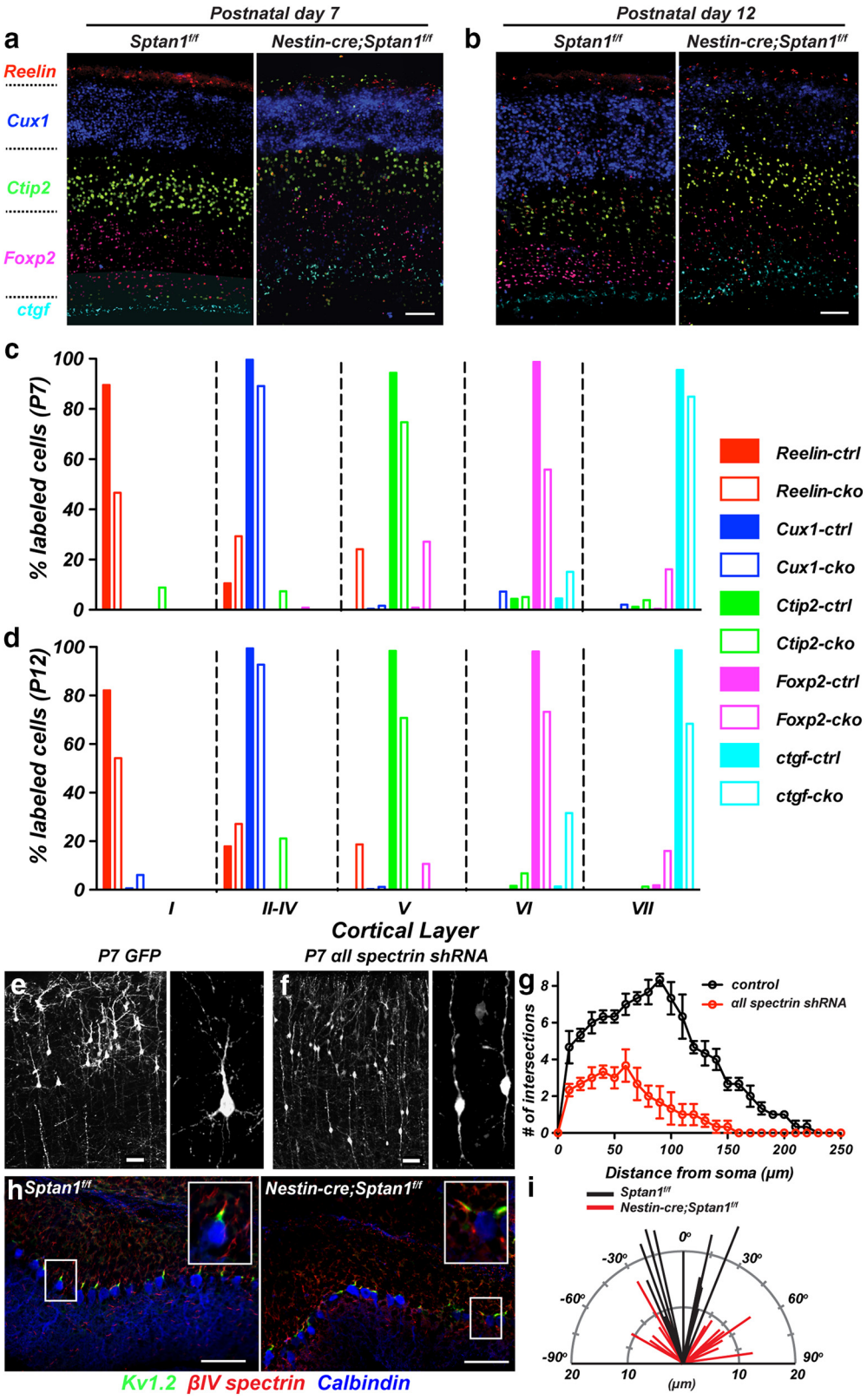

Figure 7. αII spectrin-deficient mice have disrupted cortical lamination and cerebellar organization. ***a***, ***b***, Immunostaining of cerebral cortex using antibodies against Reelin (layer I), Cux1 (layers II–IV), Ctip2 (layer V), FoxP2 (layer VI), and ctgf (subplate) at P7 (***a***) and P12 (***b***). Scale bar, 50 μm. ***c***, ***d***, Quantification of percentage of labeled cells (Reelin, red; Cux1, blue; Ctip2, green; Foxp2, magenta; ctgf, cyan) in their respective cortical layers (I, II-IV, V, VI, VII) in P7 (***c***) or P12 (***d***) control (close column) or αII spectrin-deficient (open column) cerebral cortex. ***e***, ***f***, GFP immunoreactivity in P7 rats after *in utero* electroporation using GFP alone (***e***) or GFP and αII spectrin shRNA (***f***) plasmids. Scale bar, 50 μm. ***g***, Sholl analysis of dendritic complexity in control or αII spectrin-deficient hippocampal neurons *in vitro* ($n = 3$). Error bars indicate ± SEM. ***h***, Immunostaining of P18 *Sptan1*$^{f/f}$ and *Nestin-cre;Sptan1*$^{f/f}$ cerebella using antibodies against Kv1.2 (green), βIV spectrin (red), and calbindin (blue). Scale bar, 50 μm. ***i***, Orientation and length of Purkinje neuron AIS in *Sptan1*$^{f/f}$ and *Nestin-cre;Sptan1*$^{f/f}$ mice.

specific αII/β spectrin combinations to nervous system function in distinct cell types (e.g., neurons and glia) and may be complicated by the ability of β spectrins to substitute for one another (Ho et al., 2014).

αII spectrin forms a periodic cytoskeleton with βIV spectrin at the AIS and nodes of Ranvier

Among the β spectrins, one of the most extensively studied in the vertebrate nervous system is βIV spectrin because it is highly enriched at AIS and nodes of Ranvier (Berghs et al., 2000; Komada and Soriano, 2002). Previous studies in mice demonstrated the ability of αII spectrin to coimmunoprecipitate both βIVΣ1 and βIVΣ6 (Uemoto et al., 2007) and experiments in zebrafish larvae revealed a transient localization of αII spectrin to nodes of Ranvier (Voas et al., 2007). However, βIV spectrin's function at AIS and nodes remained enigmatic for the following reasons: (1) αII spectrin has not been shown at AIS or nodes of mature axons, (2) the major βIV spectrin splice variant found in mature AIS and nodes (βIVΣ6; Yoshimura et al., 2016) lacks the canonical actin and αII spectrin-binding domains (SR1-2), and (3) loss of βIV spectrin can be partially compensated for by βI spectrin (Ho et al., 2014). Our results help to resolve these problems. First, we found that detergent extraction of unfixed, cultured hippocampal neurons reveals a detergent insoluble pool of αII spectrin restricted to the AIS. Superresolution microscopy shows that AIS αII spectrin exists in a periodic distribution with a spacing of ~190 nm, corresponding to the expected length of a spectrin tetramer (Shotton et al., 1979). Second, we showed that αII spectrin can bind to both βIVΣ1 and βIVΣ6, albeit with different affinities. Remarkably, in addition to SR1-2, we found that SR14-15, the same domain in βIV spectrin that binds to ankG (Yang et al., 2007), can also bind to αII spectrin. It will be interesting to determine whether the addition of ankG results in cooperative or competitive binding. Finally, loss of αII spectrin disrupts AIS and nodes (Huang et al., 2017), demonstrating the requirement for the spectrin cytoskeleton in their assembly and function.

Why does loss of αII spectrin cause seizures in the *Nestin-cre;Sptan1*$^{f/f}$ mice? It is possible that disrupted AIS in *Nestin-cre;Sptan1*$^{f/f}$ mice causes seizures because the AIS is the main determinant of the output of a neuron and is responsible for the initiation of axonal action potentials (Kole et

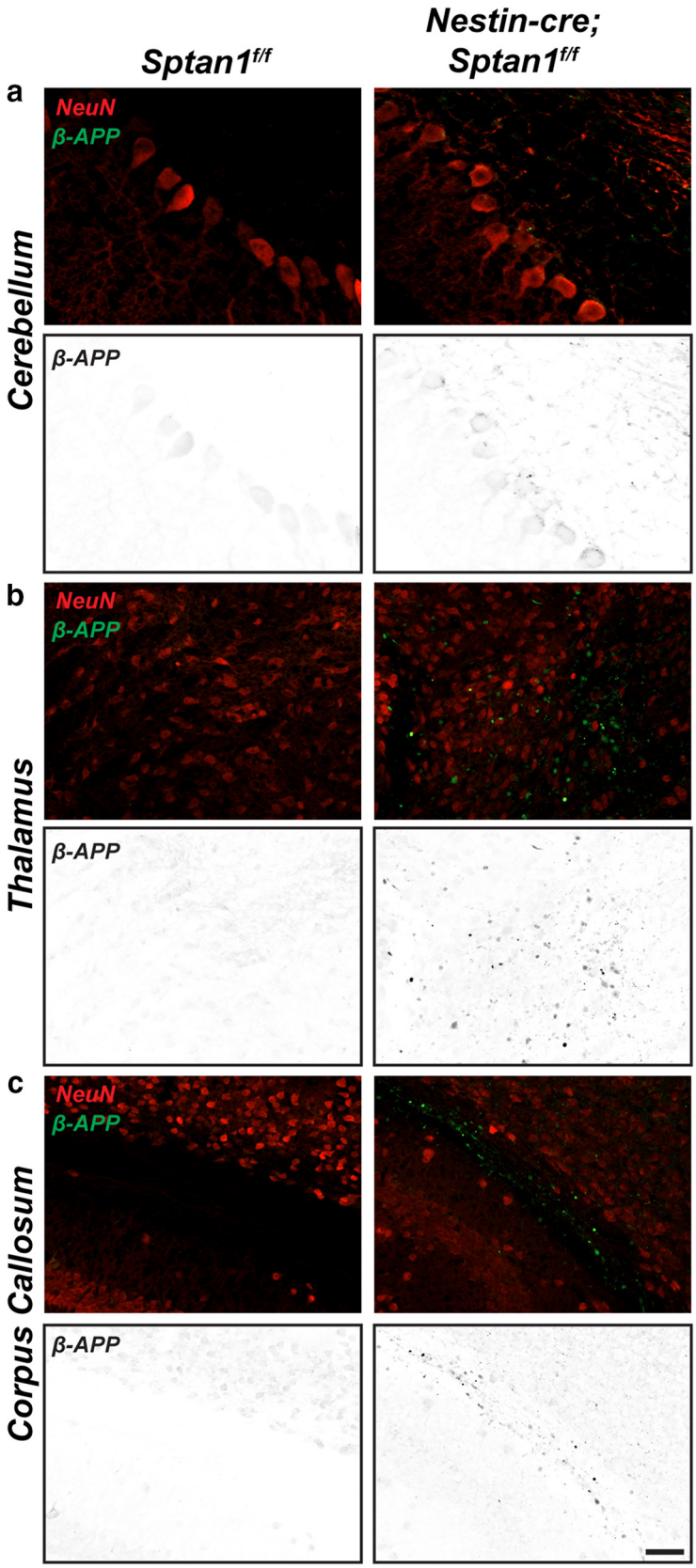

Figure 8. *Nestin-cre;Sptan1*$^{f/f}$ mice have widespread axon degeneration. ***a–c***, Immunostaining of cerebellum (***a***), thalamus (***b***), and corpus callosum (***c***) in *Sptan1*$^{f/f}$ and *Nestin-cre;Sptan1*$^{f/f}$ mice using antibodies against β-APP (green) and NeuN (red). Scale bar, 50 μm.

al., 2008). However, because both excitatory and inhibitory neurons have AIS, our experiments cannot distinguish between the contributions to seizures from excitatory or inhibitory neurons. In addition, the severely disrupted cortical lamination observed in the *Nestin-cre;Sptan1*$^{f/f}$ mice may also contribute to seizures. We found that loss of αII spectrin impaired the migration of cortical neurons to their proper locations. We speculate that, because αII spectrin plays important roles in regulating the surface expression of membrane proteins and cell adhesion molecules (Susuki et al., 2011), migration may be arrested due to an impaired response to guidance cues. This view is consistent with the observation that the axons of *Nestin-cre;Sptan1*$^{f/f}$ Purkinje neurons have significantly altered trajectories. This may reflect an impaired ability of axons to respond to guidance cues because of a loss or reduction in their receptors.

In addition to their roles in maintaining ion channel clusters at AIS, neuronal spectrins have been proposed to help axons withstand the mechanical forces to which they are exposed (Xu et al., 2013). Although the experiments described here do not test this idea directly, the observation that loss of the spectrin cytoskeleton results in widespread axon degeneration is consistent with this model. More direct evidence will require experiments that uncouple the contribution of AIS and dendritic αII spectrin from their role in long axons.

References

Bennett V, Baines AJ (2001) Spectrin and ankyrin-based pathways: metazoan inventions for integrating cells into tissues. Physiol Rev 81:1353–1392. Medline

Berghs S, Aggujaro D, Dirkx R Jr, Maksimova E, Stabach P, Hermel JM, Zhang JP, Philbrick W, Slepnev V, Ort T, Solimena M (2000) betaIV spectrin, a new spectrin localized at axon initial segments and nodes of ranvier in the central and peripheral nervous system. J Cell Biol 151:985–1002. CrossRef Medline

D'Este E, Kamin D, Balzarotti F, Hell SW (2017) Ultrastructural anatomy of nodes of Ranvier in the peripheral nervous system as revealed by STED microscopy. Proc Natl Acad Sci U S A 114:E191–E199. CrossRef Medline

Galiano MR, Jha S, Ho TS, Zhang C, Ogawa Y, Chang KJ, Stankewich MC, Mohler PJ, Rasband MN (2012) A distal axonal cytoskeleton forms an intra-axonal boundary that controls axon initial segment assembly. Cell 149:1125–1139. CrossRef Medline

Gentleman SM, Nash MJ, Sweeting CJ, Graham DI, Roberts GW (1993) Beta-amyloid precursor protein (beta APP) as a marker for axonal injury after head injury. Neurosci Lett 160:139–144. CrossRef Medline

Guerrini R, Dobyns WB (2014) Malformations of cortical development: clinical features and genetic causes. Lancet Neurol 13:710–726. CrossRef Medline

Hedstrom KL, Xu X, Ogawa Y, Frischknecht R, Seidenbecher CI, Shrager P, Rasband MN (2007) Neurofascin assembles a specialized extracellular matrix at the axon initial segment. J Cell Biol 178:875–886. CrossRef Medline

Hedstrom KL, Ogawa Y, Rasband MN (2008) AnkyrinG is required for maintenance of the axon initial segment and neuronal polarity. J Cell Biol 183:635–640. CrossRef Medline

Ho TS, Zollinger DR, Chang KJ, Xu M, Cooper EC, Stankewich MC, Bennett V, Rasband MN (2014) A hierarchy of ankyrin-spectrin complexes clusters sodium channels at nodes of Ranvier. Nat Neurosci 17:1664–1672. CrossRef Medline

Huang CY, Zhang C, Zollinger DR, Leterrier C, Rasband MN (2017) An αII spectrin based cytoskeleton protects large diameter myelinated axons from degeneration.

Ikeda Y, Dick KA, Weatherspoon MR, Gincel D, Armbrust KR, Dalton JC, Stevanin G, Dürr A, Zühlke C, Bürk K, Clark HB, Brice A, Rothstein JD, Schut LJ, Day JW, Ranum LP (2006) Spectrin mutations cause spinocerebellar ataxia type 5. Nat Genet 38:184–190. CrossRef Medline

Jungmann R, Avendaño MS, Woehrstein JB, Dai M, Shih WM, Yin P (2014) Multiplexed 3D cellular super-resolution imaging with DNA-PAINT and Exchange-PAINT. Nat Methods 11:313–318. CrossRef Medline

Knierim E, Gill E, Seifert F, Morales-Gonzalez S, Unudurthi SD, Hund TJ, Stenzel W, Schuelke M (2017) A recessive mutation in beta-IV-spectrin (SPTBN4) associates with congenital myopathy, neuropathy, and central deafness. Hum Genet 136:903–910. CrossRef Medline

Kole MH, Ilschner SU, Kampa BM, Williams SR, Ruben PC, Stuart GJ (2008) Action potential generation requires a high sodium channel density in the axon initial segment. Nat Neurosci 11:178–186. CrossRef Medline

Komada M, Soriano P (2002) βIV-spectrin regulates sodium channel clustering through ankyrin-G at axon initial segments and nodes of Ranvier. J Cell Biol 156:337–348. CrossRef Medline

Lacas-Gervais S, Guo J, Strenzke N, Scarfone E, Kolpe M, Jahkel M, De Camilli P, Moser T, Rasband MN, Solimena M (2004) BetaIVSigma1 spectrin stabilizes the nodes of Ranvier and axon initial segments. J Cell Biol 166:983–990. CrossRef Medline

Legendre K, Safieddine S, Küssel-Andermann P, Petit C, El-Amraoui A (2008) alphaII-betaV spectrin bridges the plasma membrane and cortical lattice in the lateral wall of the auditory outer hair cells. J Cell Sci 121:3347–3356. CrossRef Medline

Leterrier C, Potier J, Caillol G, Debarnot C, Rueda Boroni F, Dargent B (2015) Nanoscale architecture of the axon initial segment reveals an organized and robust scaffold. Cell Rep 13:2781–2793. CrossRef Medline

Ogawa Y, Schafer DP, Horresh I, Bar V, Hales K, Yang Y, Susuki K, Peles E, Stankewich MC, Rasband MN (2006) Spectrins and ankyrinB constitute a specialized paranodal cytoskeleton. J Neurosci 26:5230–5239. CrossRef Medline

Ogawa Y, Oses-Prieto J, Kim MY, Horresh I, Peles E, Burlingame AL, Trimmer JS, Meijer D, Rasband MN (2010) ADAM22, a Kv1 channel-interacting protein, recruits membrane-associated guanylate kinases to juxtaparanodes of myelinated axons. J Neurosci 30:1038–1048. CrossRef Medline

Olivetti PR, Maheshwari A, Noebels JL (2014) Neonatal estradiol stimulation prevents epilepsy in Arx model of X-linked infantile spasms syndrome. Sci Transl Med 6:220ra212. CrossRef Medline

Parkinson NJ, Olsson CL, Hallows JL, McKee-Johnson J, Keogh BP, Noben-Trauth K, Kujawa SG, Tempel BL (2001) Mutant beta-spectrin 4 causes auditory and motor neuropathies in quivering mice. Nat Genet 29:61–65. CrossRef Medline

Perrotta S, Gallagher PG, Mohandas N (2008) Hereditary spherocytosis. Lancet 372:1411–1426. CrossRef Medline

Rust MJ, Bates M, Zhuang X (2006) Sub-diffraction-limit imaging by stochastic optical reconstruction microscopy (STORM). Nat Methods 3:793–795. CrossRef Medline

Saitsu H, et al. (2010) Dominant-negative mutations in alpha-II spectrin cause West syndrome with severe cerebral hypomyelination, spastic quadriplegia, and developmental delay. Am J Hum Genet 86:881–891. CrossRef Medline

Schafer DP, Jha S, Liu F, Akella T, McCullough LD, Rasband MN (2009) Disruption of the axon initial segment cytoskeleton is a new mechanism for neuronal injury. J Neurosci 29:13242–13254. CrossRef Medline

Shotton DM, Burke BE, Branton D (1979) The molecular structure of human erythrocyte spectrin: biophysical and electron microscopic studies. J Mol Biol 131:303–329. CrossRef Medline

Siman R, Baudry M, Lynch G (1984) Brain fodrin: substrate for calpain I, an endogenous calcium-activated protease. Proc Natl Acad Sci U S A 81:3572–3576. CrossRef Medline

Speicher DW, Weglarz L, DeSilva TM (1992) Properties of human red cell spectrin heterodimer (side-to-side) assembly and identification of an essential nucleation site. J Biol Chem 267:14775–14782. Medline

Stankewich MC, Cianci CD, Stabach PR, Ji L, Nath A, Morrow JS (2011) Cell organization, growth, and neural and cardiac development require alphaII-spectrin. J Cell Sci 124:3956–3966. CrossRef Medline

Susuki K, Raphael AR, Ogawa Y, Stankewich MC, Peles E, Talbot WS, Rasband MN (2011) Schwann cell spectrins modulate peripheral nerve myelination. Proc Natl Acad Sci U S A 108:8009–8014. CrossRef Medline

Susuki K, Chang KJ, Zollinger DR, Liu Y, Ogawa Y, Eshed-Eisenbach Y, Dours-Zimmermann MT, Oses-Prieto JA, Burlingame AL, Seidenbecher CI, Zimmermann DR, Oohashi T, Peles E, Rasband MN (2013) Three mechanisms assemble central nervous system nodes of Ranvier. Neuron 78:469–482. CrossRef Medline

Tohyama J, Nakashima M, Nabatame S, Gaik-Siew C, Miyata R, Rener-Primec Z, Kato M, Matsumoto N, Saitsu H (2015) SPTAN1 encephalopathy: distinct phenotypes and genotypes. J Hum Genet 60:167–173. CrossRef Medline

Uemoto Y, Suzuki S, Terada N, Ohno N, Ohno S, Yamanaka S, Komada M (2007) Specific role of the truncated betaIV-spectrin Sigma6 in sodium channel clustering at axon initial segments and nodes of ranvier. J Biol Chem 282:6548–6555. CrossRef Medline

Voas MG, Lyons DA, Naylor SG, Arana N, Rasband MN, Talbot WS (2007) alphaII-spectrin is essential for assembly of the nodes of Ranvier in myelinated axons. Curr Biol 17:562–568. Medline

Writzl K, Primec ZR, Stražišar BG, Osredkar D, Pečarič-Meglič N, Kranjc BS, Nishiyama K, Matsumoto N, Saitsu H (2012) Early onset West syndrome with severe hypomyelination and coloboma-like optic discs in a girl with SPTAN1 mutation. Epilepsia 53:e106–110. CrossRef Medline

Xu K, Zhong G, Zhuang X (2013) Actin, spectrin, and associated proteins form a periodic cytoskeletal structure in axons. Science 339:452–456. CrossRef Medline

Yang Y, Lacas-Gervais S, Morest DK, Solimena M, Rasband MN (2004) BetaIV spectrins are essential for membrane stability and the molecular organization of nodes of Ranvier. J Neurosci 24:7230–7240. CrossRef Medline

Yang Y, Ogawa Y, Hedstrom KL, Rasband MN (2007) βIV spectrin is recruited to axon initial segments and nodes of Ranvier by ankyrinG. J Cell Biol 176:509–519. CrossRef Medline

Yoshimura T, Stevens SR, Leterrier C, Stankewich MC, Rasband MN (2016) Developmental changes in expression of βIV spectrin splice variants and axon initial segments and nodes of Ranvier. Front Cell Neurosci 10:304. CrossRef Medline

Zhang Y, Chen K, Sloan SA, Bennett ML, Scholze AR, O'Keeffe S, Phatnani HP, Guarnieri P, Caneda C, Ruderisch N, Deng S, Liddelow SA, Zhang C, Daneman R, Maniatis T, Barres BA, Wu JQ (2014) An RNA-sequencing transcriptome and splicing database of glia, neurons, and vascular cells of the cerebral cortex. J Neurosci 34:11929–11947. CrossRef Medline

Zhong G, He J, Zhou R, Lorenzo D, Babcock HP, Bennett V, Zhuang X (2014) Developmental mechanism of the periodic membrane skeleton in axons. eLife 3.